

Received 13 January 2004  
Accepted 20 September 2004

# High-resolution strain mapping in bulk samples using full-profile analysis of energy-dispersive synchrotron X-ray diffraction data

A. Steuwer,<sup>a\*</sup> J. R. Santisteban,<sup>b</sup> M. Turski,<sup>a</sup> P. J. Withers<sup>a</sup> and T. Buslaps<sup>c</sup>

<sup>a</sup>Manchester Materials Science Centre, University of Manchester, Grosvenor Street, Manchester M1 7HS, UK, <sup>b</sup>Department of Materials Engineering, Open University, Milton Keynes MK7 1AA, UK, and <sup>c</sup>European Synchrotron Radiation Facility, rue J. Horowitz, Grenoble, France.

Correspondence e-mail: steuwer@ill.fr

© 2004 International Union of Crystallography  
Printed in Great Britain – all rights reserved

The feasibility of both high spatial and strain resolution is demonstrated using high-energy X-rays between 100 and 300 keV on beamline ID15A at the ESRF. The data analysis was performed using a multiple-peak Pawley-type refinement on the recorded spectra. An asymmetric peak profile was necessary in order to obtain a point-to-point uncertainty of  $10^{-5}$ . The measurements have been validated with complementary techniques or reference data.

## 1. Introduction

In this paper, we report the results of strain mapping experiments on bulk engineering components with high spatial and strain resolution using energy-dispersive synchrotron X-ray diffraction (EDXRD) and full-profile analysis. Bulk in this context is taken to represent sample volumes that are usually considered inaccessible to X-rays.

This method has been applied to the investigation of the residual strain fields in two typical engineering components where there are potentially great benefits to be gained, namely around a fatigue crack in a 25 mm thick austenitic stainless-steel compact tension (CT) specimen, and in a titanium linear-friction weld (LFW). Both problems are considered unsuitable for similar investigations by neutron diffraction: in the former case, because of the high spatial resolution required, and in the latter case, because titanium is a relatively poor neutron scatterer. We show that strain mapping by EDXRD can be efficiently undertaken in both cases. The spatial resolution achieved was 0.2 mm, but this is not limited by the beam geometry but by the average size (and hence number) of diffracting grains in the sampling volume. A strain resolution of the order  $10^{-5}$  was routinely achieved by using a Pawley-type full-pattern refinement with an asymmetric peak profile. The photon energy range used in the experiment reached 300 keV, which (together with the high flux available at the ESRF) provides penetration depths of several cm in most engineering materials. At such high energies, inelastic (*e.g.* Compton) scattering becomes increasingly important. The use of high X-ray energies is normally accompanied by relatively small diffraction angles (in our case  $2\theta \simeq 3.5^\circ$ ), which leads to considerable elongation of the gauge volume. This limits the applicability somewhat to essentially two-dimensional problems (Brusch, 1998).

## 1.1. Background

Energy-dispersive synchrotron X-ray diffraction is a versatile and powerful tool for materials research, providing full X-ray spectra at a single diffraction angle (Liss *et al.*, 2003). The possibility of separating the spectra of different phases allows the simultaneous study of phase strains in composite materials, with the same advantages as time-of-flight (TOF) neutron diffraction. On the other hand, the combination of high flux and excellent beam definition offers the prospect of high spatial resolution with short counting times, opening up a whole new range of possible applications, ranging from basic materials engineering to dynamic *in situ* measurements.

Energy-dispersive strain measurements have tended to be focused on near-surface regions (Brusch & Reimers, 1998), intergranular studies that do not require strain mapping or single-peak analysis for strain mapping of bulk components (Croft *et al.*, 2002; Kuntz, Wadley & Black, 1993; Honkimäki & Suortti, 1992; Pyzalla, 2000; Korsunsky *et al.*, 2002; Pyzalla & Reimers, 2003; Reimers *et al.*, 1999). In many cases it has proven difficult to attain the benchmark  $10^{-4}$  accuracy within reasonable data acquisition timescales considered optimal for engineering strain measurements. This has been interpreted as an inherent uncertainty attributed to the comparatively broad widths of the observed peaks, which stems from the limited energy resolution of current detectors, as well as limitations in electronic data-acquisition hardware (Korsunsky *et al.*, 2002; Otto, 1997) and microstructure (Kuntz *et al.*, 1993).

When considering accurate peak location it should be borne in mind that energy-dispersive profiles typically comprise asymmetric peaks (Wilson, 1973; Knoll, 1989; Otto, 1997). However, the appropriateness of the traditional Gaussian/Lorentzian/pseudo-Voigtian profiles in full-pattern refinement has received little attention [one exception being the work of *e.g.* Ballirano & Caminiti (2001)]. Furthermore, there are potentially great benefits to be gained by undertaking full-

pattern analysis of the type routinely used on pulsed-source neutron diffraction instruments (Larson & Von Dreele, 2000) in terms of shorter acquisition times, better grain sampling statistics and the averaging over many reflections to negate the influence of elastic and plastic anisotropy as well as texture (Daymond *et al.*, 1997). It is encouraging that uncertainties in determining the lattice parameter of similar magnitude to that required for strain measurements have been found by EDXRD during high-pressure experiments using a novel type of pattern-fitting code (Dong *et al.*, 2003).

## 2. The experiment

### 2.1. Experimental setup

The experiments were conducted on the high-energy beamline ID15A at the European Synchrotron Research Facility (ESRF) in Grenoble, France. This beamline is capable of producing a high-flux beam with energies up to several hundreds of keV (Tschentscher & Suorrti, 1998). The detector was a liquid-nitrogen-cooled germanium single-crystal detector attached to a multi-channel analyser (MCA) set at 4096 channels. The maximum energy was set at approximately 300 keV and calibrated with a radioactive source, the known spectral emission of which was fitted with a second-order polynomial  $E_i = a_1 + a_2\Delta_i + a_3\Delta_i^2$  to convert the channel element  $\Delta_i$  to energy  $E_i$ . The detector was placed at approximately  $2\theta = 3.5^\circ$ . The calibrated conversion constants are  $\{a_1, a_2, a_3\} = \{0.94262, 0.0725129, 4.49035 \times 10^{-8}\}$ , which results in a detector resolution (channel width) of 73 eV at 100 keV. The small second-order coefficient indicates that the conversion is almost linear. For a cubic lattice parameter of around 3.6 Å (for austenitic f.c.c. steels) this configuration places the lowest reflection at around 100 keV, at which point the attenuation was sufficiently low to allow the work to be undertaken in non-symmetric transmission geometry even for relatively thick samples, see *e.g.* Fig. 4. On the one hand, this has the advantage that the direction of strain measurement is almost perpendicular to the incident and diffracted beam, which simplifies the positioning of the sample (placed with its face normal parallel to the incident beam). On the other hand, this is accompanied by a very elongated gauge volume. For residual strain measurements, only the relative change of the lattice parameter across the sample is of interest, and no attempts have been made at calibration during the experiment

to obtain an absolute measure (beyond the first or second significant digit) of the lattice parameter. The incident-beam geometry was defined by a pair of vertical and horizontal slits, and the apertures varied for the different samples. The diffracted beam was shaped by two sets of static slits, one close to the sample with a horizontal gap of 100 µm and another slit close to the detector with a horizontal gap of 400 µm. The vertical beam geometry was defined by the vertical gap of the incident slits only. Between the slits, the beam travelled through a copper tube shielded with lead. Additional slabs of lead were moulded around the detector window to prevent the entry of background radiation. A schematic of the experimental setup is shown in Fig. 1.

### 2.2. Cracked austenitic stainless-steel specimen

Crack growth rates generally increase as a crack lengthens; thus the majority of the lifetime of a crack in a structural component is spent when the crack is short. Uncertainties in short crack-propagation behaviour therefore have the greatest influence on lifetime prediction. Unfortunately, this is also the regime within which the study of crack behaviour is most difficult. Furthermore, it is well known that near the surface (plane stress) crack behaviour is very different from in the bulk (plane strain), necessitating the study of relatively thick samples if the bulk triaxial stress state is of interest (Knott, 1973). Uncertainty leads to conservatism in engineering design and may result in unnecessary repair of structures in which the early stages of cracking are identified in service. This is expensive both in financial and efficiency terms. Better models for the early stages of crack nucleation are therefore required, and these must be verified by experimental observations. High-resolution EDXRD promises a significant breakthrough in the study of cracks. Since the characteristic stress field around the crack tip is estimated to decay within a few tens to hundreds of micrometres, outside the range of what is achievable with neutrons, EDXRD is currently the only candidate for the non-destructive characterization of strain fields in bulk engineering materials with such spatial resolution.

The sample material, austenitic steel of type 316H, was kindly provided by British Energy Plc., UK, and is a commonly used engineering stainless steel with a composition of mainly Fe, 17%Cr, and 11%Ni with minor additions of Mo and Mb. This alloy has a relatively low yield (0.2% proof) stress of around 200 MPa, but relatively high ultimate tensile stress of around 500 MPa. Several nominally identical specimens (labelled CT1 to CT5) were cut to a standard compact-tension (CT) geometry; see Fig. 2. A 25 mm sample thickness was chosen in order to generate a triaxial stress state within the bulk. It is reasonable to assume that the residual strain field at mid-thickness is approximately ‘plane strain’, which allows the use of an elongated gauge volume (inevitable at high energy). A residual stress field was generated in four samples by preloading by compressing each sample beyond yield at the points indicated, and then releasing the applied force. This plastically deforms the material locally around the

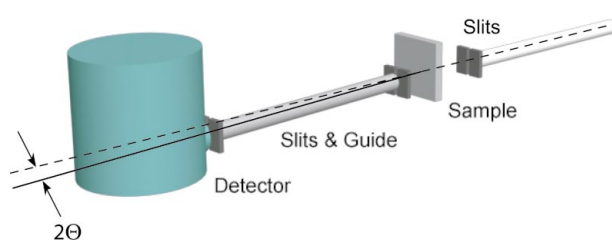


**Figure 1**

The basic experimental setup. The direction of strain measurement (parallel to the scattering vector) lies in the horizontal plane, almost perpendicular to the incident and diffracted beams.

notch. Upon removal of the applied force, the plastically deformed notch regions become residually tensively stressed in the direction of the applied preload. In one sample (labelled CT1) a 0.5 mm wide and 1 mm long pre-crack was electro-discharged machined at the notch, from which a fatigue crack of 2 mm length was introduced. One sample was left undeformed in order to have an unstressed reference specimen. The typical grain size in this material is between 50 and 100  $\mu\text{m}$ . The sample was mounted on a translation stage and placed in the calibrated rotation centre of the experimental setup. An area of  $14 \times 10$  mm has been mapped with a gauge volume defined by  $0.4 \times 0.4$  mm incident-beam geometry at  $2\theta = 3.5^\circ$ , with the scattering vector (the direction of strain measured) parallel to the initial loading direction. The length of the resulting gauge volume was approximately 15 mm. Counting times were 50 s per point. The total map consisted of around 800 measurements points, which is equivalent to around 20 h of counting time.

### 2.3. Titanium linear-friction weld

Linear-friction welding (LFW) is a direct-drive friction-welding technique, where the frictional heat is generated by the linear relative motion of the parts to be joined (see Fig. 2). This technique offers an attractive method of joining turbine blades to disks in aero-engines, thus creating an integrally bladed disk, or ‘blisk’, at relatively low cost compared with an all-machined structure. Manufacturing companies all over the world have developed a keen interest in this joining method, because it is seen as a key technology for the next generation of lighter, more efficient and more environmentally friendly jet engines, partly through its unequalled ability to join different materials as well as materials that are difficult to weld. Titanium, for example, has a great affinity for oxygen,

nitrogen and hydrogen, to which exposure during the welding process can cause embrittlement. The specimen material was the so-called IMI-550 titanium alloy, with a typical composition of titanium and approximately 4 wt% Al, 4% Mo, 2% Sn and 0.55% Si. This material is frequently used in the aero-engine industry, because of its attractive mechanical properties and excellent corrosion behaviour. The room temperature proof stress (0.2%) is around 959 MPa, and its tensile strength around 1104 MPa. The alloy is a two-phase material, with a dominant hexagonal ( $\alpha$ ) and a minority cubic ( $\beta$ ) phase (see §4.2). The weld and heat-affected zone are typically of the scale of a few mm, and the microstructure is known to vary markedly over this range (Preuss *et al.*, 2003; Daymond & Bonner, 2003). Although non-destructive strain determination by neutron diffraction can in principle be carried out on this type of weld (Daymond & Bonner, 2003), the poor scattering properties of titanium (very small coherent scattering length) and vanadium (almost no coherent scattering) require the use of costly and time-consuming experiments. As we demonstrate in this paper, high-energy synchrotron diffraction promises significant improvements. The sample geometry is  $13 \times 26 \times 65$  mm, with the weld plane at the centre of the long axis (see Fig. 2). The beam size in this experiment was set at  $0.2 \times 0.2$  mm, and the sample was scanned across the weld line with the scattering vector parallel to the weld plane and parallel to the friction sliding direction. Along this direction, one expects the residual strains to be strongly tensile in the weld region. The counting time per spectrum was 40 s. The sample was scanned across the weld line using a step size of 0.2 mm in the weld region and 1 mm in the parent material. In total, 70 measurements were made in this line scan over a period of less than 1 h.

### 3. Data preprocessing and analysis

The results presented in this paper were prepared using a Pawley (Pawley, 1981) or LeBail refinement approach, using the software package GSAS (Larson & Von Dreele, 2000) in LeBail-type extraction mode. Although GSAS is intrinsically able to perform refinement on energy-dispersive data, it only provides a Gaussian peak profile for its analysis. However, it is well known that the peak profiles in EDXRD spectra are of asymmetric nature (Wilson, 1973; Knoll, 1989; Honkimäki, 1996; Otto, 1997). This asymmetry can be seen in the difference curves of Figs. 3 and 4, and was observed to increase with energy. In our approach, the collected EDXRD spectra were transformed to an artificial reciprocal scale, essentially equivalent to that of time-of-flight, and then stored in GSAS RALF format using logarithmic rebinning, which then allows the use of the asymmetric peak profile (No. 3) developed for

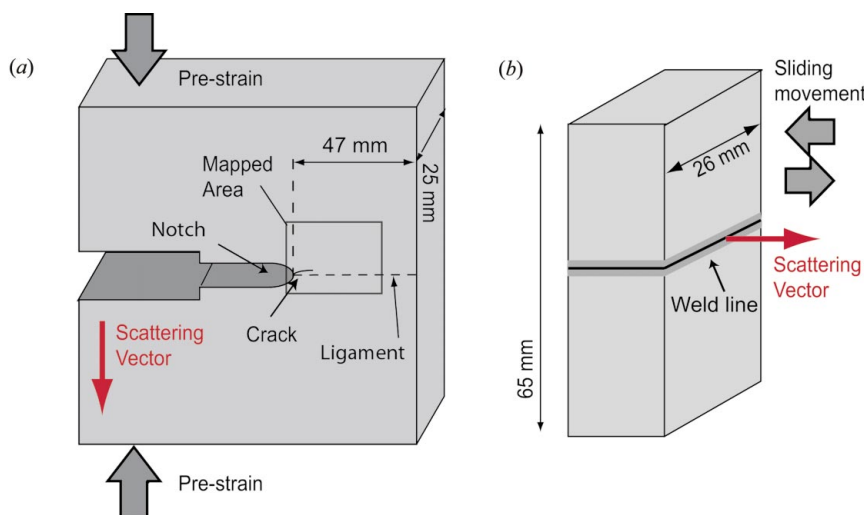


**Figure 2**

A schematic of the samples: on the left (a), the austenitic CT specimen, showing the location of the fatigue crack, and the remaining uncracked ligament, the location of the compressive preload and the mapped area; on the right (b), the titanium linear-friction-welded sample. Also indicated is the direction of the relative movement of the pieces during the welding processes. In both cases, the scattering vector indicates the direction in which strains were measured.

TOF neutron diffraction in GSAS. A similar approach, but using a transformation to the angular dispersive domain, has been adopted and reported by Ballirano & Caminiti (2001) in the refinement of energy-dispersive diffraction data acquired on a laboratory X-ray source. The (slowly varying) Compton scattering contribution is assumed to be included in the refinement of general background. Our approach was driven by the observation that although the individual peak fittings, as well as Pawley refinements of the data in the energy domain, achieved reasonable fits with very good lattice-parameter uncertainties (of the order  $10^{-6}$ ), the resulting strain profiles were relatively poor (very large point-to-point scatter of the order  $10^{-3}$ ). These were not consistent with possible intergranular strains, but could be attributed to an inappropriate peak profile and, to a certain degree, to instrumental effects encountered at such small diffraction angles.

A detailed discussion of the data conversion algorithm and analysis is beyond the scope of this paper and will be presented at a later stage. Needless to say that the use of inappropriate profiles leads to much larger peak position uncertainties. It is worthwhile noting here that given the very good counting statistics displayed (e.g. in Fig. 3) in terms of background, width and integrated intensity of the observed peaks, a peak position uncertainty of the order  $\Delta d/d \simeq 10^{-5}$  is in line with expectation following the arguments of Withers *et al.* (2001) with respect to peak position uncertainties.

## 4. Results

### 4.1. Austenitic steel CT specimen

Fig. 5 shows the elastic opening strain in the vicinity of the crack tip. The strain uncertainty per measurement point is typically of the order of  $\Delta a/a \simeq 5 \times 10^{-5} = 50 \mu\epsilon$ . The experimental data in Fig. 5 can be directly compared with the

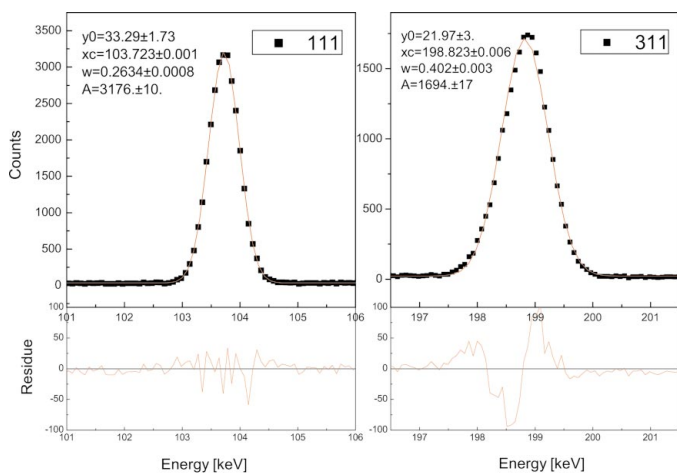


**Figure 3**

Two diffraction peaks and fits to a simple Gaussian (expressed in ‘amplitude’ form), in this case the Fe 111 and Fe 311 reflections of the CT specimen. The quantities  $y_0$ ,  $x_c$ ,  $w$  and  $A$  denote the background, peak centre, peak width and amplitude, respectively. The difference curves at the bottom highlight the profile asymmetry (increasing with energy).

prediction of finite element (FE) analysis for approximately the same volume element, shown in Fig. 6. The white semi-circular object represents the pre-machined notch. There is a 2 mm region of very small tensile strains at the beginning of the fatigue crack, and very high tensile strains around the crack tip. FEA and experiment display the same characteristics of the tensile strain field in both the near-crack region as well as further away from the crack.

Fig. 7 compares the longitudinal elastic strain across the sample from the notch to the back face. Shown are the results of EDXRD in the fatigue-cracked sample, the uncracked sample, and a reference sample measured with neutron diffraction, alongside the predictions from the three-dimensional finite-element analysis.

The neutron diffraction results were obtained with a gauge volume of approximately  $(1.5 \text{ mm})^3$ , and the steep strain gradient near the notch is lost due to spatial averaging within the gauge volume. In contrast, the corresponding synchrotron data show a steep tensile strain gradient towards the notch, in

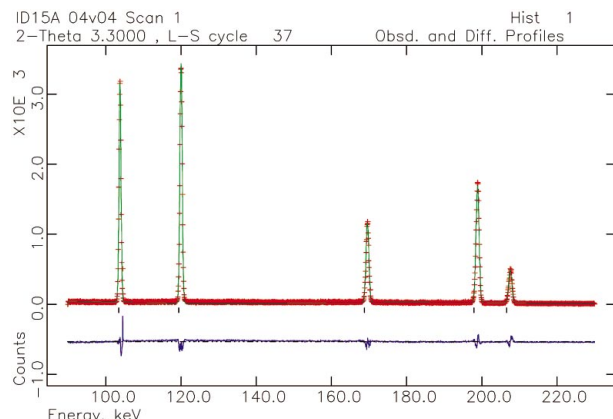


**Figure 4**

A typical refined EDXRD spectrum of the CT steel specimen in the energy domain. Only the part of the spectrum visible in the figure (the five lowest reflections) has been used in the refinement. The difference curve indicates the use of an inappropriate Gaussian profile function.

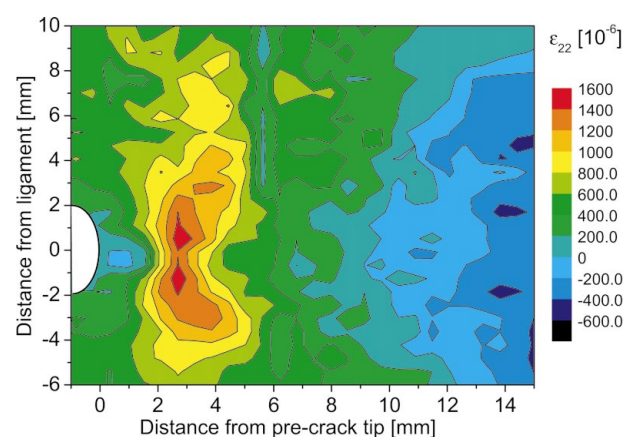


**Figure 5**

The elastic strain  $\varepsilon_{22}$  measured in the vicinity of the crack tip for specimen CT1. The apparent vertical feature in the centre of the sample (at 6 mm) is due to missed data points when spectra were lost during a beam refill.

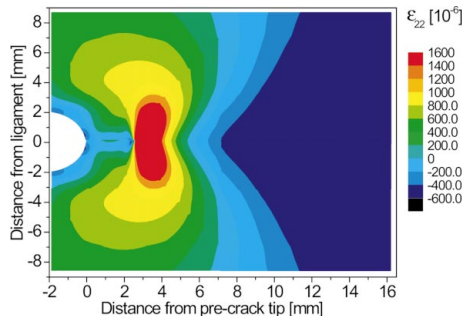
agreement with the FE analysis for the uncracked specimen. The presence of the crack in the specimen CT1 can be inferred from the fact that in the wake of the crack the strain is negligible, whereas immediately ahead of the crack tip, a

strong tensile residual strain field exists. The correlation between the neutron and synchrotron results on nominally identical samples in the region away from the crack is very good.

#### 4.2. Titanium linear-friction weld

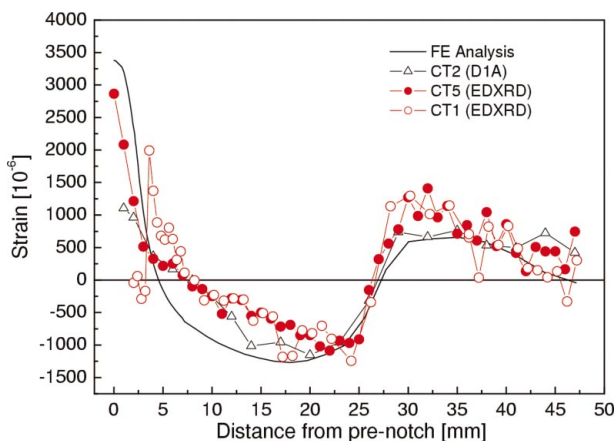
Fig. 8 shows a typical spectrum of the titanium linear friction weld. The resolution is sufficient to see a clear separation of the two phases (marked with  $\alpha$  and  $\beta$ ). Fig. 9 shows the strain profile measured across the weld line expressed for each lattice parameter and phase individually. The strain uncertainty is typically  $80 \mu\epsilon$  in the  $\alpha$  phase and twice as large for the minority  $\beta$  phase. The measured strain profile is in very good agreement with expectations and results reported by Daymond & Bonner (2003). In essence, the strains in the heat-affected zone (there is no fusion zone for LFW) are tensile due to the localized heating and plastic deformation. These stresses extend approximately 2 mm either side of the weld. The observed profiles differ slightly due to the effect of strong elastic and plastic anisotropy during the strong deformation experienced. A more detailed discussion of the effects of the linear friction welding process on the microstructure, as well as its correlation on the peak profiles, is beyond the scope of this paper.

Fig. 10 shows the change in the diffraction pattern in the immediate vicinity of the weld line. From this it is clear that there is a dramatic change in the microstructure over a distance of approximately 0.2–0.3 mm at the weld line, where the joining process induces dynamic recrystallization with very fine grains and strong deformation texture due to the extreme thermo-mechanical deformation experienced in the plasticized zone on either side of the weld line. This is reflected in the sharp rise in intensity of the 110 diffraction peak of the  $\alpha$  phase at 140 keV (or  $1.45 \text{ \AA}$ ), and the corresponding depletion of other reflections, as well as the minority  $\beta$  phase. The whole-pattern refinement is able to cope with the extreme



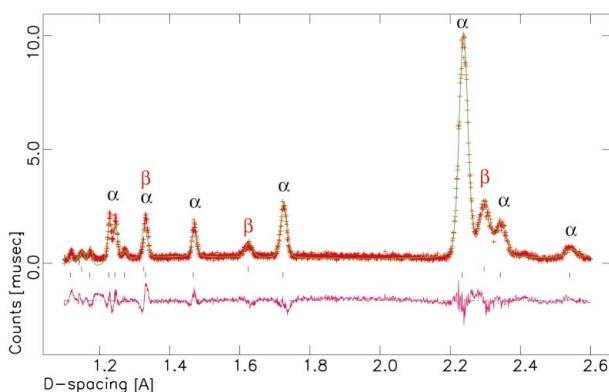
**Figure 6**

The elastic opening strain  $\varepsilon_{22}$  as predicted by the three-dimensional finite-element analysis for a cracked specimen (CT1).



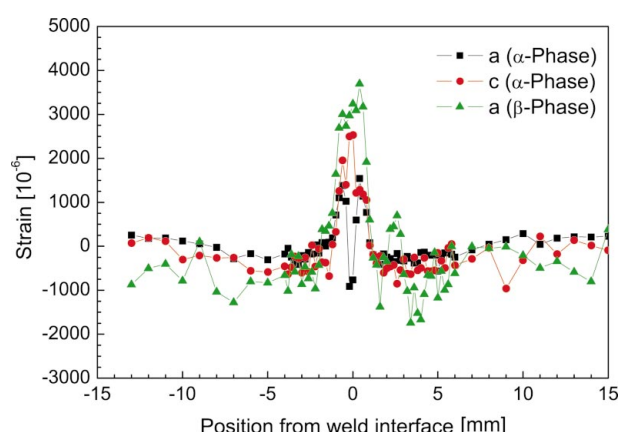
**Figure 7**

A comparison of the elastic strain  $\varepsilon_{22}$  across the crack plane at mid-thickness. Shown are the predictions from a three-dimensional finite-element model for an uncracked specimen, the EDXRD results for the fatigue-cracked sample (CT1) and the uncracked sample (CT5), and neutron diffraction data collected on D1A at the ILL.



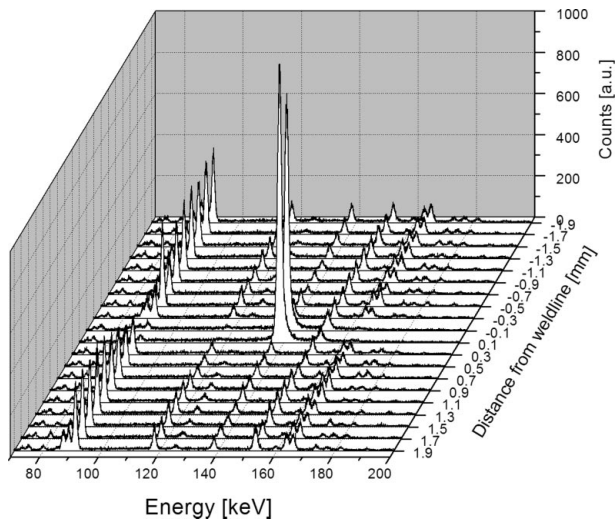
**Figure 8**

The EDXRD spectrum of the IMI-550 linear-friction-welded sample after re-binning and fitting. Note the contributions from the two phases indicated by the peak position markers between the fitted spectrum and the difference curve at the bottom.



**Figure 9**

The residual strains (parallel to the sliding direction) across the weld line for the two phases in IMI550. The discontinuity in lattice-parameter behaviour of the  $\alpha$  phase at the weld line is due to the extreme texture that the material exhibits very locally, reminiscent of that of a single crystal.

**Figure 10**

A graph showing the evolution of the diffraction spectra across the weld line. The sharp rise in intensity of the 110 peak at 140 keV indicates the strong texture at the weld line.

change in relative peak strength and provide a reliable measure of elastic strain across the whole weld test-piece.

## 5. Discussion and conclusion

We have demonstrated the ability to use a full-pattern fitting technique on energy-dispersive synchrotron X-ray diffraction data for strain scanning on relatively thick engineering components made of steel and a titanium alloy, with high spatial resolution and at very high rates of data acquisition compared with neutron diffraction. It was found that for the slit settings used an asymmetric peak profile significantly improved the strain profile characterization and uncertainty. A point-to-point lattice-strain resolution of the order  $10^{-5}$  was routinely achieved for the steel sample and dominant phase in IMI550, and could be further improved using better peak profiles. However, the exact profile depends amongst other factors on the particular slit configuration employed. This accuracy could not be achieved using single-peak analysis with a symmetric profile for which the point-to-point scatter was in excess of  $10^{-3}$ . A spatial resolution of 0.2 mm laterally has been achieved, but was essentially limited by the specimen microstructure, not the beam geometry. In other words, the achievable spatial resolution is limited by the grain size, as the beam size should be at least of the same order. Additionally, we would like to highlight the fact that a certain amount of divergence of the beam, as well as working at high energies, which gives rise to larger Ewald spheres (Liss *et al.*, 2003), increases the probability of satisfying the Bragg condition for diffraction. This allows the presented whole-pattern fitting approach to push the boundary of spatial resolution to essentially ‘few-grain sampling’. The investigated thicknesses of 25 mm for both the steel and titanium samples by no means represent the limits of this technique on ID15A. It is straightforward to apply this method to other materials and environments, where *e.g.* the fast data acquisition times allow

dynamic *in situ* investigations (a common application being high-pressure anvil cells) or buried interfaces. The penetration at high X-ray energies is accompanied by a considerable elongation of the gauge volume due to the low scattering angles. This must be taken into account in the preparation and evaluation of the experiment. The collected spectra display relatively low background, and in the chosen configuration most fluorescence peaks occurred at energies lower than the lowest diffraction peaks. By fitting the diffraction spectrum using a Pawley-type refinement with an asymmetric peak profile we have been able to reduce the point-to-point scatter markedly, partly by improved fit and partly by sampling more diffracting grains. Excellent agreement has been achieved with the neutron diffraction data, which samples more grains because of the larger gauge volume and higher incident beam divergence in the case of the (un)cracked austenitic steel. In the case of the linear friction weld, the method was able to detect and cope with the very marked change in crystallographic texture in the mechanically affected weld zone. As usual when converting measured lattice spacings into strains, a precise knowledge of the unstrained lattice spacing is essential, which may not be constant for all measurement points and may vary *e.g.* around a weld. However, this problem is generic to strain scanning techniques based on diffraction and has been discussed on several occasions in the literature (Hauk, 1997; Noyan & Cohen, 1987). This method has the potential to enhance strain measurements on engineering alloys significantly, even in relatively thick sections, particularly in situations where the stress field varies sharply in two dimensions, such as in some cases around cracks. It is worth mentioning here that by using two or more solid-state detectors simultaneously at different azimuthal angles (which is straightforward to implement), one could measure several directions of strain at the same time, thus greatly increasing the efficient use of beam time. Such a set-up can potentially simplify the experiment significantly, *e.g.* if it involves large pieces of equipment which are not easily rotated such as tensile rigs.

*Note added in proof:* Further experimental evidence has emerged since the submission of this manuscript, whereby a spatial resolution of 20  $\mu\text{m}$  in a very finely grained ( $\sim 1 \mu\text{m}$ ) material was achieved at similar strain accuracy, but with a significantly reduced asymmetry in the observed peaks, due to the much narrower slit opening required for such spatial resolution. [A very good fit could in fact be achieved by a pseudo-Voigtian profile (Steuwer, 2004)].

The authors express their gratitude to Drs A. M. Korsunsky, V. Honkimäki, T. J. Marrow and R. B. Cernik for advice and discussions, and to Drs S. Bray of Rolls & Royce Plc., UK, and P. J. Bouchard of British Energy Plc., UK, for providing the specimen. PJW acknowledges the Royal Society–Wolfson Merit award. AS acknowledges the hospitality of the FaME38 facility at the ESRF-ILL, Grenoble. The authors acknowledge the access to synchrotron X-rays at the European Synchrotron Radiation Facility (ESRF) through proposals ME279, ME452, ME667, as well as neutron beam time at the Institute Laue-Langevin (ILL) through proposal No. 7-01-111.

## References

- Ballirano, P. & Caminiti, R. (2001). *J. Appl. Cryst.* **34**, 757–762.
- Brusch, G. (1998). Dissertation, Hahn-Meitner-Institut, Berlin, Germany.
- Brusch, G. & Reimers, W. (1998). *Proceedings of the International Conference on Residual Stress ICRS5*, pp. 557–562.
- Croft, M., Zakharchenko, I., Zhong, Z., Gurlak, Y., Hastings, J., Hu, J., Holtz, R., DaSilva, M. & Tsakalakos, T. (2002). *J. Appl. Phys.* **92**, 578–586.
- Daymond, M. R. & Bonner, N. W. (2003). *Physica B*, **325**, 130–137.
- Daymond, M. R., Bourke, M. A. M. & Von Dreele, R. B. (1997). *J. Appl. Phys.* **82**, 1554–1562.
- Dong, Y. H., Liu, J., Li, Y.-C. & Li, X.-D. (2003). *J. Appl. Cryst.* **36**, 1123–1127.
- Hauk, V. (1997). *Structural and Residual Stress Analysis by Nondestructive Methods*. Amsterdam: Elsevier.
- Honkimäki, V. (1996). *J. Appl. Cryst.* **29**, 617–624.
- Honkimäki, V. & Suortti, P. (1992). *J. Appl. Cryst.* **25**, 97–104.
- Knoll, G. E. (1989). *Radiation Detection and Measurement*, 2nd ed. New York: John Wiley.
- Knott, J. F. (1973). *Fundamentals of Fracture Mechanics*. London: Butterworth.
- Korsunsky, A. M., Collins, S. P., Owen, R. A., Daymond, M. R., Saïda, A. & James, K. A. (2002). *J. Synchrotron Rad.* **9**, 77–81.
- Kuntz, T., Wadley, H. & Black, D. (1993). *Metall. Trans. A*, **24**, 1117–1126.
- Larson, A. C. & Von Dreele, R. B. (2000). Los Alamos National Laboratory Report LAUR 86-748.
- Liss, K. D., Bartels, A., Schreyer, A. & Clemens, H. (2003). *Text. Microstruct.* **35**, 219–252.
- Noyan, I. C. & Cohen, J. B. (1987). *Residual Stress – Measurement by Diffraction and Interpretation*. New York: Springer.
- Otto, J. W. (1997). *J. Appl. Cryst.* **30**, 1008–1015.
- Pawley, G. S. (1981). *J. Appl. Cryst.* **14**, 357–361.
- Preuss, M., Fonseca, J., Wang, L., Steuwer, A., Withers, P. J. & Bray, S. (2003). *International Ti Conference Hamburg 14–19 July, 2003*.
- Pyzalla, A. (2000). *J. Nondestr. Eval.* **19**, 21–31.
- Pyzalla, A. & Reimers, W. (2003). In *Analysis of Residual Stress by Diffraction using Neutron and Synchrotron Radiation*, edited by M. E. Fitzpatrick & A. Lodini. London: Taylor and Francis.
- Reimers, W., Pyzalla, A., Broda, M., Brusch, G., Dantz, D., Schmackers, T. & Liss, K.-D. (1999). *J. Mater. Sci. Lett.* **18**, 581–583.
- Steuwer, A. (2004). In preparation.
- Tschentscher, T. & Suortti, P. (1998). *J. Synchrotron Rad.* **5**, 286–292.
- Wilson, A. J. C. (1973). *J. Appl. Cryst.* **6**, 230–237.
- Withers, P. J., Daymond, M. R. & Johnson, M. W. (2001). *J. Appl. Cryst.* **34**, 737–743.